

the induction of associative LTP. Such a role is also supported by recent experiments with a caged function-blocking antibody to BDNF (36), although the site of BDNF release is not clear yet. Although an autocrine action of postsynaptically released neurotrophin-4/5 has been proposed for the neuromuscular junction (2), there is evidence for an activity-dependent release of BDNF from presynaptic terminals in cortical neurons (37). A recent report (38) provides evidence for activity-dependent postsynaptic release of BDNF from cultured hippocampal neurons. However, because this BDNF release has not yet been directly correlated with LTP recordings, more work is required to determine whether, during LTP induction, BDNF is released from either pre- or postsynaptic compartments, or even from both compartments together.

Whatever the site of BDNF release, our results show that a brief BDNF pulse and a weak afferent burst robustly elicited LTP. Like tetanus-induced LTP (16, 17), the induction of BDNF-mediated LTP required postsynaptic  $Ca^{2+}$  signaling (39) and NMDA receptor activation, as well as a close temporal association of pre- and postsynaptic activity. The mutual occlusion between BDNF-mediated and tetanus-evoked LTP suggests shared expression mechanisms. However, our results do not exclude a presynaptic expression of the BDNF-mediated LTP and are, therefore, not necessarily in contradiction with earlier evidence stressing the contribution of presynaptic mechanisms. An important conclusion of the present study is that spiny dendrites of mature dentate granule cells represent a highly responsive compartment for the rapid BDNF action. The block of this responsiveness prevented the induction of BDNF-mediated LTP. Our results reveal a critical mechanism underlying the surprisingly rapid, LTP-inducing action of BDNF and support an instructive role for BDNF in the induction of LTP in the mature brain.

References and Notes

1. H. Thoenen, *Science* **270**, 593 (1995).
2. A. F. Schinder, M.-m. Poo, *Trends Neurosci.* **23**, 639 (2000).
3. E. M. Schuman, *Curr. Opin. Neurobiol.* **9**, 105 (1999).
4. A. M. Lohof, N. Y. Ip, M.-m. Poo, *Nature* **363**, 350 (1993).
5. H. Kang, E. M. Schuman, *Science* **267**, 1658 (1995).
6. N. T. Sherwood, D. C. Lo, *J. Neurosci.* **19**, 7025 (1999).
7. A. F. Schinder, B. Berninger, M.-m. Poo, *Neuron* **25**, 151 (2000).
8. E. Messaoudi, K. Bardsen, B. Srebro, C. R. Bramham, *J. Neurophysiol.* **79**, 496 (1998).
9. M. Korte et al., *Proc. Natl. Acad. Sci. U.S.A.* **92**, 8856 (1995).
10. S. L. Patterson et al., *Neuron* **16**, 1137 (1996).
11. M. Korte et al., *Proc. Natl. Acad. Sci. U.S.A.* **93**, 12547 (1996).
12. A. Figurov, L. D. Pozzo-Miller, P. Olafsson, T. Wang, B. Lu, *Nature* **381**, 706 (1996).
13. H. Kang, A. A. Welcher, D. Shelton, E. M. Schuman, *Neuron* **19**, 653 (1997).
14. G. Chen, R. Kolbeck, Y. A. Barde, T. Bonhoeffer, A. Kossel, *J. Neurosci.* **19**, 7983 (1999).
15. L. Minichiello et al., *Neuron* **24**, 401 (1999).
16. B. Gustafsson, H. Wigström, *Trends Neurosci.* **11**, 156 (1988).

17. R. C. Malenka, J. A. Kauer, R. S. Zucker, R. A. Nicoll, *Science* **242**, 81 (1988).
18. B. Xu et al., *J. Neurosci.* **20**, 6888 (2000).
19. J. N. Jovanovic, A. J. Czernik, A. A. Fienberg, P. Greengard, T. S. Sihra, *Nature Neurosci.* **3**, 323 (2000).
20. W. Gottschalk, L. D. Pozzo-Miller, A. Figurov, B. Lu, *J. Neurosci.* **18**, 6830 (1998).
21. L. D. Pozzo-Miller et al., *J. Neurosci.* **19**, 4972 (1999).
22. M. Frerking, R. C. Malenka, R. A. Nicoll, *J. Neurophysiol.* **80**, 3383 (1998).
23. T. Tanaka, H. Saito, N. Matsuki, *J. Neurosci.* **17**, 2959 (1997).
24. E. S. Levine, C. F. Dreyfus, I. B. Black, M. R. Plummer, *Proc. Natl. Acad. Sci. U.S.A.* **92**, 8074 (1995).
25. H. E. Scharfman, *J. Neurophysiol.* **78**, 1082 (1997).
26. For electrophysiological methods used, see supplementary information on Science Online at www.sciencemag.org/cgi/content/full/295/5560/1729/DC1. All critical control experiments of the specificity of the rapid BDNF action performed previously for CA1 pyramidal cells (27) were repeated in dentate granule cells in hippocampal slices from adult mice and are also available on Science Online at the same address.
27. K. W. Kafitz, C. R. Rose, H. Thoenen, A. Konnerth, *Nature* **401**, 918 (1999).
28. Y. Kovalchuk, J. Eilers, J. Lisman, A. Konnerth, *J. Neurosci.* **20**, 1791 (2000).
29. P. Andersen, B. Holmqvist, P. E. Voorhoeve, *Acta Physiol. Scand.* **66**, 448 (1966).
30. For LTP experiments, afferent medial perforant path fibers were stimulated in the middle molecular layer at a frequency of 0.06 Hz, and synaptic responses were recorded in the voltage-clamp mode at a holding potential of  $-75$  to  $-80$  mV. After a stable baseline recording was obtained (for up to 20 min), LTP was induced by switching the amplifier to current-clamp mode and pairing the BDNF ejection pulse lasting for 300 to 600 ms with a burst stimulation (five or six stimuli at 50 Hz). The burst stimulation was delivered 50 ms before the end of the ejection pulse to ensure the coincidence of the synaptic responses with the moment of maximal concentration of BDNF at the synaptic site. Such pairing successfully evoked LTP even when executed once. Routinely, however, pairing was produced twice with an interval of 20 s to obtain a nearly saturating level of potentiation. It is noteworthy that such a BDNF-

pairing protocol induced LTP also in hippocampal CA1 pyramidal cells [Web fig. 5 (26)]. Experiments in which the series resistance ( $R_s$ ) was less than 20 megohms or in which  $R_s$  changed by more than 15% during the recording period were discarded. All data are expressed as mean  $\pm$  SEM.

32. T. V. Bliss, T. Lomo, *J. Physiol. (London)* **232**, 331 (1973).
32. E. Hanse, B. Gustafsson, *J. Neurosci.* **12**, 3226 (1992).
33. Loading of perforant path axons and dentate granule cells with a  $Ca^{2+}$ -indicator dye was performed according to the protocol described in detail by Wu and Saggau (41) following a procedure pioneered by Regehr and Tank (42). Briefly, as indicated schematically in Fig. 5C, an Oregon BAPTA-1-AM (Molecular Probes, Inc., Eugene, OR) (0.9 mM in 10% dimethyl sulfoxide and 1% pluronic acid)-containing micropipette was positioned 100 to 200  $\mu$ m below the slice surface into the molecular layer. After releasing dye by gentle-pressure application for about 30 s into the slice, the micropipette was withdrawn. This procedure yielded a robust and reproducible loading of axons far away from the site of dye ejection ( $>1$  mm) and a dendritic loading of tens of granule cells.
34. B. U. Keller, A. Konnerth, Y. Yaari, *J. Physiol. (London)* **435**, 275 (1991).
35. Addition of 1 or 10 mM BAPTA to the pipette solution prevented LTP induction in six out of six granule cells.
36. A. H. Kossel, S. B. Cambridge, U. Wagner, T. Bonhoeffer, *Proc. Natl. Acad. Sci. U.S.A.* **98**, 14702 (2001).
37. K. Kohara, A. Kitamura, M. Morishima, T. Tsumoto, *Science* **291**, 2419 (2001).
38. M. Hartmann, R. Heumann, V. Lessmann, *EMBO J.* **20**, 5887 (2001).
39. H. Kang, E. M. Schuman, *Neurosci. Lett.* **282**, 141 (2000).
40. F. A. Edwards, A. Konnerth, B. Sakmann, T. Takahashi, *Pfluegers Arch. Eur. J. Physiol.* **414**, 600 (1989).
41. L. G. Wu, P. Saggau, *J. Neurosci.* **14**, 645 (1994).
42. W. G. Regehr, D. W. Tank, *J. Neurosci. Methods* **37**, 111 (1991).
43. We thank H. Thoenen, T. Bonhoeffer, O. Garaschuk, B. Gustafsson, and C. Rose for comments on early versions of the manuscript. Supported by grants from the Deutsche Forschungsgemeinschaft (A.K.).

6 November 2001; accepted 15 January 2002

## Divided by Cytochrome Oxidase: A Map of the Projections from V1 to V2 in Macaques

Lawrence C. Sincich\* and Jonathan C. Horton

Current models partition the primate visual system into dorsal (magno) and ventral (parvo, konio) streams. Perhaps the strongest evidence for this idea has come from the pattern of projections between the primary visual area (V1) and the second visual area (V2). Prior studies describe three distinct pathways: magno to thick stripes, parvo to pale stripes, and konio to thin stripes. We now demonstrate that V1 output arises from just two sources: patch columns and interpatch columns. Patch columns project to thin stripes and interpatch columns project to pale and thick stripes. Projection of interpatches to common V2 stripe types (pale and thick) merges parvo and magno inputs, making it likely that these functional channels are distributed strongly to both dorsal and ventral streams.

In primates, the pathway from the eye via the lateral geniculate nucleus to striate cortex is segregated along three lines: magnocellular, parvocellular, and koniocellular (1, 2). The

pathway from V1 to V2 is thought to perpetuate this division, by maintaining segregation of these three channels (3–5). Specifically, a magno-dominated pathway from layer 4B

REPORTS

terminates in thick stripes (6), a konio-dominated patch pathway from layer 2/3 innervates thin stripes, and a parvo-dominated interpatch pathway links layer 2/3 to pale stripes (7). These

discrete parallel channels are believed to convey visual information about motion, color, and form, respectively. V2 neurons reflect this segregation, both in their physiological properties (8–10) and in their pattern of projections to higher visual centers. Thick stripes project to area MT, a motion center in the dorsal pathway, whereas thin and pale stripes project to area V4, a form/color region in the ventral pathway (9,

11, 12). This scheme is admittedly an oversimplification (13, 14), but it prevails in our current view of the basic organization of the visual system (15–17).

The link from V1 to V2 is a major pathway through which most visual signals pass before dissemination to the rest of extrastriate cortex (18–21). By making [<sup>3</sup>H]proline injections into V1, we have shown that pale stripes receive the strongest striate input (22). We have now mapped the V1-to-V2 projections in macaque monkeys (*n* = 17) using a retrograde tracer. Contrary to prior reports, the thin, pale, and thick stripes in V2 received input from the same layers of striate cortex. More important, their V1 input was segregated by cytochrome oxidase into only two systems: patch columns or interpatch columns.

To map V1-to-V2 projections, one must identify the cytochrome oxidase stripes reliably; these are often indistinct in macaques (23). To accomplish this, we unfolded and flattened the convoluted lunate sulcus before histological processing. A section cut parallel to the flattened cortical surface, containing portions of V1 and V2 representing central vision, is shown stained for cytochrome oxidase (Fig. 1A). The stripes could be readily differentiated. They formed a repeating pale-thick-pale-thin pattern oriented perpendicular to the V1/V2 border (24). To make discrete retrograde tracer injections, we used gold-conjugated cholera toxin B subunit (CTB). This tracer resists diffusion, allowing <1-mm-diameter injections, and leaves a faint purple witness mark at injection sites (Fig. 1A, inset). This enabled one to assign each injection to a stripe type before the pattern of cytochrome oxidase staining was obscured by

Beckman Vision Center, University of California, San Francisco, San Francisco, CA 94143-0730, USA.

\*To whom correspondence should be addressed. E-mail: sincich@itsa.ucsf.edu

**Fig. 1.** V2 stripes and injection sites can be identified in flattened macaque visual cortex before transported tracer is revealed. (A) Cytochrome oxidase–stained section containing the central portions of V1 and V2, showing pale stripes between thick stripes (brackets) and thin stripes (black arrows). CTB injections appear as miniscule purple spots; three (white arrows) are squarely in thick stripes. Inset shows injection marked with an asterisk. (B) Same section, after silver enhancement of CTB, showing that none of the thick stripe injections spread into flanking pale stripes. (C) Pale stripe (white arrows) and thin stripe (arrowhead) injections from another macaque, after reaction for CTB. Dashed outlines indicate fields shown in Fig. 2. Scale bars, 2 mm.

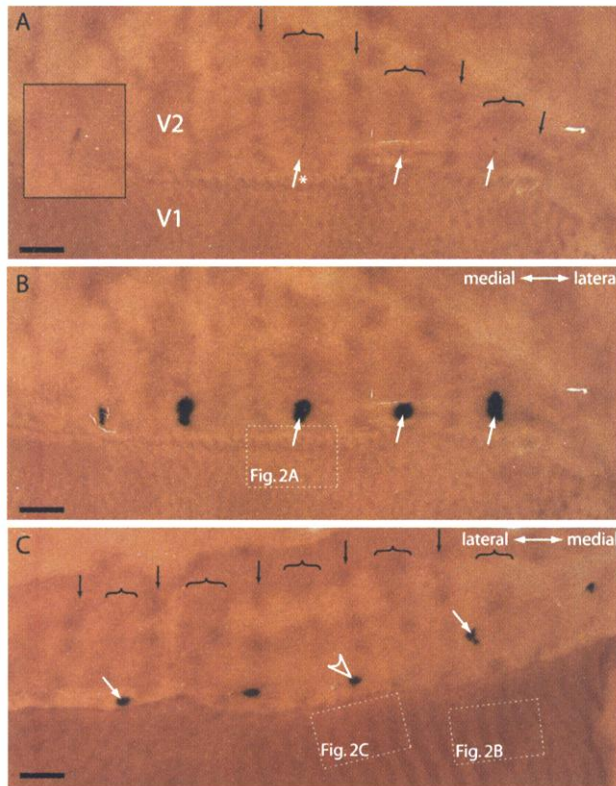
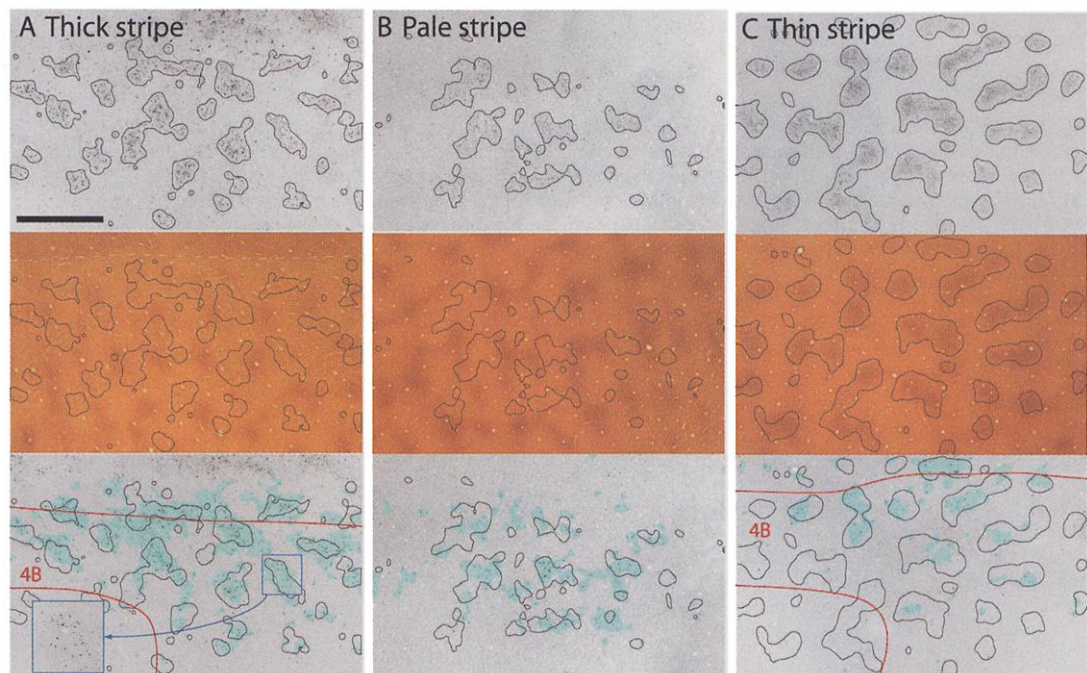


**Fig. 2.** All V2 stripes receive projections from neurons in layers 2/3 and 4B. (A) CTB labeled cells in layer 2/3 (top panel) from a thick stripe injection are outlined by computer-generated contours of the labeling (39). Middle, the same section, in bright-field, with layer 2/3 labeling clearly nestled in the cytochrome oxidase interpatch regions. Bottom, the labeling in layer 4B (shaded blue) from the same injection, with outlines superimposed from the layer 2/3 labeling. Inset, a group of 4B cells at higher magnification. (B) Cells in layer 2/3 (top) labeled after a pale stripe injection were situated in interpatches (middle) and aligned, with clusters of labeled interpatch cells in layer 4B (bottom). (C) Thin stripe injection led to patch labeling in layer 2/3 (top and middle), plus light patch labeling in layer 4B (bottom). Scale bar, 1 mm.



REPORTS

silver intensification of the conjugated gold. Stripe assignments could thus be made before the pattern of retrograde labeling in V1 was

known. Only injections confined to a clear-cut thick, pale, or thin stripe were included in our analysis ( $n = 77$ , from a total of 187 injections).

More than 100 injections were rejected because they straddled stripes, strayed into V1, were too small for detectable transport, or landed in an unidentifiable stripe.

The same section after silver intensification is shown in Fig. 1B. The retinotopic map is mirrored across the V1/V2 border, allowing one to match each V2 injection site with its field of labeled cells in V1. The lateral three injections landed squarely in thick stripes. The extent of the silver material around the injection sites provided an upper estimate of local tracer diffusion. In each case, the tracer was restricted to a thick stripe, without contamination of flanking pale stripes. One thin and two pale stripes are shown with discrete injections in another monkey (Fig. 1C).

Thick stripe injections labeled a large population of cells in layer 2/3 (Fig. 2A, top). This layer was not previously thought to project to thick stripes (6). Layer 2/3 labeling was produced by all thick stripe injections ( $n = 27$ ). The labeled neurons were localized to interpatches (Fig. 2A, middle). From the same injections, labeled neurons were also present in layer 4B (Fig. 2A, bottom) (6). However, far more cells were present in layer 2/3 than in layer 4B. The 4B neurons were also localized to interpatch regions and thus clustered directly below those in layer 2/3. Therefore, thick stripes received projections from neurons in multiple V1 layers, rather than from layer 4B exclusively, and the projection neurons were grouped into interpatch columns.

Pale stripe injections ( $n = 33$ ) showed the same pattern. Although pale stripes are twice as numerous as thick stripes, it was difficult to make injections confined to pale stripes, because they are much narrower than thick stripes. Rich labeling was found in layer 2/3 interpatches (Fig. 2B, top and middle). There was also labeling in layer 4B (Fig. 2B, bottom) in 31 of 33 injections. The 4B label was concentrated underneath layer 2/3 label, forming interpatch columns, like the projections to thick stripes.

Thin stripe injections ( $n = 17$ ) produced labeling of patches in layer 2/3 (Fig. 2C, top and middle). We also found label in layer 4B (Fig. 2C, bottom) directly beneath the labeled cells of layer 2/3, thereby defining a patch column. Among the three stripe types, thin stripes received projections from the fewest cells in layer 4B.

We hypothesized that separate interpatch cell populations might provide inputs to thick and pale stripes. Paired injections of CTB and WGA-HRP (wheat germ agglutinin conjugated to horseradish peroxidase), separated by 1.25 mm, were made into V2. In three cases we succeeded in hitting cleanly adjacent thick and pale stripes (Fig. 3, A and B) (25). The labeled fields from the two tracers partially overlapped in V1 (Fig. 3, C to E). A third of the WGA-HRP-positive cells were double-labeled, indi-

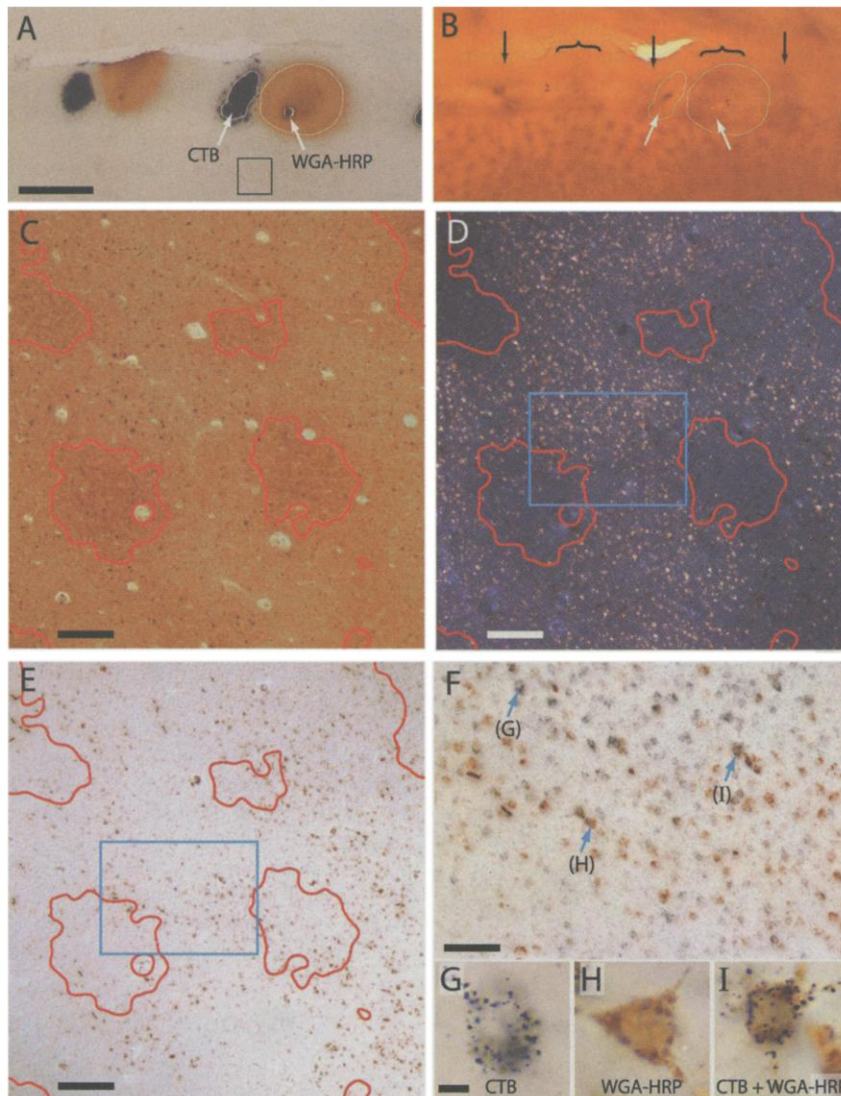
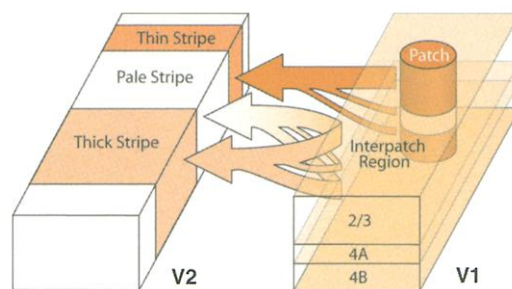


**Fig. 3.** Thick and pale stripes share input from interpatches in layer 2/3. (A) Paired injections (white outlines) of CTB and WGA-HRP showed no cross-contamination at the injection sites. The black box indicates the zone of maximum overlap between the fields of cells filled retrogradely by the two labels. (B) An adjacent cytochrome oxidase section shows that the CTB injection is in a pale stripe and the WGA-HRP injection is in a thick stripe (bracket). (C) Cytochrome oxidase section of the box in (A), outlining the patches. (D) Dark-field view of the box in (A) photographed to reveal only CTB. (E) Bright-field view with semicrossed polarizers to show only WGA-HRP. (F) An enlarged bright-field view of the blue box in (D) and (E), containing 202 labeled cells: 102 with CTB (G), 67 with WGA-HRP (H), and 33 with both tracers (I). Scale bars: 2 mm, (A and B); 100  $\mu$ m, (C to E); 50  $\mu$ m, (F); 3  $\mu$ m, (G to I).

**Fig. 4.** Projections from V1 to V2 in macaques are mainly bipartite. Schematic model showing that cells in layers 2/3, 4A, and 4B from patches project to thin stripes, whereas those from interpatches project to thick and pale stripes. Cells in layer 5/6 from patches and interpatches project to all stripe types.



cating that many V1 neurons project to both pale and thick stripes (Fig. 3, F to I). By contrast, paired tracer injections ( $n = 2$ ) in adjacent thin and pale stripes revealed virtually no double-labeled cells. Thus, the V1 projections from interpatches to pale and thick stripes arise from a common source, although most neurons do project exclusively to either a pale stripe or a thick stripe.

The V2 tracer injections revealed novel projections from other cortical layers. Layer 4A is the thinnest layer in V1 (<50  $\mu\text{m}$  thick), receives a direct projection from the parvocellular system, and has a characteristic cytochrome oxidase honeycomb pattern (26). It sent a dual pattern of projections to V2. Thick and pale stripe injections produced 4A label in interpatch columns [Web fig. 1A (27)]. Thin stripe injections resulted in 4A label that coincided with patch columns [Web fig. 1B (27)]. This projection from layer 4A adds a second potential disynaptic route from the geniculate to V2: parvocellular  $\rightarrow$  layer 4A  $\rightarrow$  V2, in addition to the known koniocellular  $\rightarrow$  patches  $\rightarrow$  V2 pathway (28). Injections in all stripes labeled numerous large neurons, often Meynert cells, near the layer 5/6 border. These cells were distributed indiscriminately with respect to patches and interpatches.

These findings recast the V1-to-V2 pathway. Previous studies found projections arising from only single layers, organized in a tripartite fashion: layer 2/3 patches  $\rightarrow$  thin stripes, layer 2/3 interpatches  $\rightarrow$  pale stripes, and layer 4B  $\rightarrow$  thick stripes (6, 7). It has subsequently been recognized that considerable mixing of magno, parvo, and konio geniculate channels occurs within V1 (29). However, the apparent existence of three distinct, partitioned V1 projections to thick, pale, and thin stripes implied that three channels—dominated by magno, parvo, and konio inputs—survived after processing within V1. We now show that thick, thin and pale stripes all receive projections from the same V1 layers: heaviest from layer 2/3 and less from layers 4A, 4B, and 5/6. The dominant theme is not tripartite, but bipartite segregation defined by cytochrome oxidase columns: patches  $\rightarrow$  thin stripes, and interpatches  $\rightarrow$  pale and thick stripes (Fig. 4). These anatomical data explain the relatively poor segregation of receptive field properties in pale and thick stripes found by some investigators (30–32). Our results provide a new connectional foundation for the cortical hierarchy of visual areas (16, 33). They suggest a rich intermingling of form, color, and motion signals between the streams bound for the dorsal “where” and ventral “what” pathways (17, 34).

References and Notes

1. R. W. Rodieck, M. Watanabe, *J. Comp. Neurol.* **338**, 289 (1993).  
 2. S. H. Hendry, R. C. Reid, *Annu. Rev. Neurosci.* **23**, 127 (2000).  
 3. M. S. Livingstone, D. H. Hubel, *Science* **240**, 740 (1988).

4. S. Zeki, S. Shipp, *Nature* **335**, 311 (1988).  
 5. A. W. Roe, D. Y. Ts'o, *Cerebral Cortex*, vol. 12, *Extrastriate Cortex in Primates*, K. S. Rockland, J. H. Kaas, A. Peters, Eds. (Plenum Press, New York, 1997), pp 295–333.  
 6. M. S. Livingstone, D. H. Hubel, *J. Neurosci.* **7**, 3371 (1987).  
 7. ———, *J. Neurosci.* **4**, 309 (1984).  
 8. D. H. Hubel, M. S. Livingstone, *J. Neurosci.* **7**, 3378 (1987).  
 9. E. A. DeYoe, D. C. Van Essen, *Nature* **317**, 58 (1985).  
 10. A. W. Roe, D. Y. Ts'o, *J. Neurosci.* **15**, 3689 (1995).  
 11. S. Shipp, S. Zeki, *Nature* **315**, 322 (1985).  
 12. E. A. DeYoe, D. J. Felleman, D. C. Van Essen, E. McClelland, *Nature* **371**, 151 (1994).  
 13. K. A. C. Martin, *Trends Neurosci.* **11**, 380 (1988).  
 14. W. H. Merigan, J. H. R. Maunsell, *Annu. Rev. Neurosci.* **16**, 369 (1993).  
 15. D. J. Felleman, D. C. Van Essen, *Cereb. Cortex* **1**, 1 (1991).  
 16. D. C. Van Essen, J. L. Gallant, *Neuron* **13**, 1 (1994).  
 17. L. G. Ungerleider, J. V. Haxby, *Curr. Opin. Neurobiol.* **4**, 157 (1994).  
 18. F. A. Mettler, *J. Comp. Neurol.* **61**, 221 (1935).  
 19. H. G. J. M. Kuypers, M. K. Szwarcbart, M. Mishkin, H. E. Rosvold, *Exp. Neurol.* **11**, 245 (1965).  
 20. B. G. Cragg, *Vision Res.* **9**, 733 (1969).  
 21. S. M. Zeki, *Brain Res.* **14**, 271 (1969).  
 22. L. C. Sincich, J. C. Horton, *J. Comp. Neurol.*, in press (2002).  
 23. Experiments were conducted in adult macaques (7 *Macaca mulatta* and 10 *M. fascicularis*) by using surgical procedures approved by the UCSF Committee on Animal Research and in accordance with NIH guidelines. Pressure injections of ~140 nl 1% CTB (List Biological Laboratories, Campbell, CA) spaced 5.5 mm apart were made along the posterior lip of the lunule sulcus in both hemispheres. Injections were made blindly with respect to cytochrome oxidase stripe type and location. Monocular enucleation was performed in 11 animals to delineate ocular dominance columns in V1. No difference in the projection pattern was observed between enucleated and control animals. After 3 to 7 days for transport, the animals were killed with pentobarbital (150 mg/kg) and perfused transcardially with 1% paraformaldehyde. The cortex was flattened (35), sectioned tangentially at 50  $\mu\text{m}$ , slide mounted, and processed for cytochrome oxidase histochemistry (36). Assignment of V2 stripe type for each injection was made before CTB was visualized by silver enhancement with the IntenSE-M kit. Intensification was performed by two 30-min rinses in 0.1 M sodium acetate solution, 25 min in IntenSE-M, 30 min in sodium acetate, and 40 min in fresh IntenSE-M before a brief rinse and coverslipping.  
 24. R. B. H. Tootell, M. S. Silverman, R. L. De Valois, G. H. Jacobs, *Science* **220**, 737 (1983).  
 25. A pressure injection of 40 nl of 4% WGA-HRP was placed 1.25 mm lateral to each CTB injection. Processing for CTB and WGA-HRP was performed in free-floating sections. CTB was reacted as above, with the addition of a 5-min exposure to a 2% sodium thiosulfate solution after silver enhancement. WGA-HRP was then reacted according to a tetramethylbenzidine-ammonium molybdate protocol (37) followed by diaminobenzidine stabilization (38). Selected V1 fields 380  $\times$  260  $\mu\text{m}$  located in regions of maximum tracer overlap were examined at 400 $\times$  to count each WGA-HRP, CTB, and double-labeled cell.  
 26. J. C. Horton, *Philos. Trans. R. Soc. London B. Biol. Sci.* **304**, 199 (1994).  
 27. Supplementary material is available on Science Online at [www.sciencemag.org/cgi/content/full/295/5560/1734/DC1](http://www.sciencemag.org/cgi/content/full/295/5560/1734/DC1)  
 28. S. H. Hendry, T. Yoshioka, *Science* **264**, 575 (1994).  
 29. E. M. Callaway, *Annu. Rev. Neurosci.* **21**, 47 (1998).  
 30. E. Peterhans, R. von der Heydt, *Eur. J. Neurosci.* **5**, 509 (1993).  
 31. J. B. Levitt, D. C. Kiper, J. A. Movshon, *J. Neurophysiol.* **71**, 2517 (1994).  
 32. K. R. Gegenfurtner, D. C. Kiper, S. B. Fenstemaker, *Vis. Neurosci.* **13**, 161 (1996).  
 33. M. P. Young, *Nature* **358**, 152 (1992).  
 34. L. Krubitzer, J. Kaas, *Vis. Neurosci.* **5**, 609 (1990).  
 35. J. F. Olavarria, D. C. Van Essen, *Cereb. Cortex* **7**, 395 (1997).  
 36. M. T. T. Wong-Riley, *Brain Res.* **171**, 11 (1979).  
 37. S. LeVay, T. Voigt, *Exp. Brain Res.* **82**, 77 (1990).  
 38. D. B. Rye, C. B. Saper, B. H. Wainer, *J. Histochem. Cytochem.* **32**, 1145 (1984).  
 39. Cells labeled with CTB in sections stained for cytochrome oxidase were photographed through crossed Polaroid filters with dark-field illumination, by using a cooled charge-coupled device (CCD) camera. Images were digitally inverted. Contour plots of label density were made with custom software written in Matlab 5.0. Contours were selected after the following image processing steps: subtracting a low-pass Fourier-filtered version of the image (cutoff frequency = 8 cyc/mm), thresholding at 3 SD above the mean image gray-level, blurring with a gaussian kernel ( $\sigma_{1/2} = 45 \mu\text{m}$ ).  
 40. Supported by grants EY10217 (J.C.H.), EY13676 (L.C.S.), and EY02162 (Beckman Vision Center) from the National Eye Institute. Support was also received from That Man May See, The Bunter Fund, and Research to Prevent Blindness (Lew Wasserman Merit Award to J.C.H.). We thank D. Adams, S. Hendry, and J. Kaas for comments on the manuscript and D. Hocking for technical assistance.

9 November 2001; accepted 15 January 2002

## Placebo and Opioid Analgesia—Imaging a Shared Neuronal Network

Predrag Petrovic,<sup>1</sup> Eija Kalso,<sup>2</sup> Karl Magnus Petersson,<sup>1</sup> Martin Ingvar<sup>1\*</sup>

It has been suggested that placebo analgesia involves both higher order cognitive networks and endogenous opioid systems. The rostral anterior cingulate cortex (rACC) and the brainstem are implicated in opioid analgesia, suggesting a similar role for these structures in placebo analgesia. Using positron emission tomography, we confirmed that both opioid and placebo analgesia are associated with increased activity in the rACC. We also observed a covariation between the activity in the rACC and the brainstem during both opioid and placebo analgesia, but not during the pain-only condition. These findings indicate a related neural mechanism in placebo and opioid analgesia.

Placebo analgesia is an important component in pain management (1), although the basic mechanisms are still poorly understood. At

least some aspects of placebo analgesia are dependent upon endogenous opioid systems (1–3) because the effect may be partly abol-